A Computational Analysis of Ground Effect Influence on a Transonic/Supersonic Projectile

Cameron J. Sheridan*

University of New South Wales at Australian Defence Force Academy, Canberra

The ground effect (GE) experienced by transonic/supersonic projectiles flying close to solid surfaces has been the subject of a significant research program at the University of New South Wales over the past several years. The present study examines how a nearby ground surface influences the aerodynamic forces and moments acting on a transonic/supersonic projectile in the range of $M_\infty = 1.1$–1.5. This is done by means of a numerical analysis and a number of wind-tunnel tests conducted for both qualitative and quantitative validation. Experimental data has previously revealed different phenomena that occur over a range of ground clearances with the observed behaviour changing as the Mach number is varied. Different shock reflection configurations have been shown to develop for particular combinations of ground clearance and Mach number. The potential of the ground plane to induce a suction force on the projectile was found to cease to exist once the projectile reaches or exceeds $M_\infty = 1.5$. The GE was also found to have an appreciable influence on other important flow field features including the bow shock stand-off distance, Mach stem height, wake distortion/deflection, and the pressure distribution along the projectiles surface.

Nomenclature

α	Angle of attack, [deg]
ζ_L	Lift influence potential (positive area under lift curve)
ζ_S	Suction influence potential (negative area under lift curve)
μ	Mach angle, [deg]
C_D	Coefficient of drag in the flow direction, based on projected frontal area
C_L	Coefficient of lift, based on planform area (away from ground $+ve$)
C_M	Pitching moment coefficient about projectile CG ($+ve$ nose down)
C_P	Coefficient of pressure
d	Projectile diameter [mm]
GE	Ground Effect
h	Height above the ground plane [mm]
h/d	Ground separation distance
l	Projectile length [mm]
M_∞	Free-stream Mach number
MS/h	Mach-stem height
SD/d	Shock stand-off ratio
x/l	Non-dimensional station along projectile

*PLTOFF, School of Engineering and Information Technology, ZEIT4500/4501

I. Introduction

A. Background and Motivation

THE behavior of projectiles when travelling at transonic and supersonic speeds in close proximity to a solid surface has been investigated over the past several years as part of a significant research program at the University of New South Wales. Tests have been extensively conducted by means of live-fire range for transonic[1] and supersonic[2] regimes (see Fig. 1). The scientific community has recognised significant importance of this field to military applications such as close-combat urban environments, missiles entering low-level flight, and military aircraft release weapon stores mechanisms. Study has also been concentrated towards the design of land-speed record vehicles[3] and racing vehicles[4] in the subsonic regime. The latter discussed the effect of an inverted aerofoil-shaped front wing as it creates a suction force on the body - strength dependent on ground separation distance - due to the Venturi effect. In the same way, the lift force generated may be normal to the ground. Lift and suction both have benefits in Formula One design in order to vary the friction drag that is experienced by the tyres. The influence of GE depends upon on M_∞, h/d, and geometry. For more complex geometries such as aircraft, GE occurs within the region of approximately one characteristic length (in this case, the chord of the wing) from the ground plane. Such close proximity is not uncommon for contemporary transomnic jets. Near ground flying is advantageous for aircraft as a means to generate additional lift and improve its stealth by remaining unseen by potential enemy radar.

Unlike both aircraft and racing vehicles where it is quite difficult to examine the actual influence the ground plane has on the body, a projectile in ground effect is unique in that at an angle of attack of α=0° the axisymmetric body is unable to generate any lift or pitching moment by itself; therefore any observed changes in both the surrounding flowfield and aerodynamic parameters are solely attributable to being within close proximity to a solid surface, *i.e.* GE. Although this investigation only examines the effects of a transonic/supersonic projectile in GE, the conclusions drawn may be applicable in design considerations of future missile and related armament development. For particular flow conditions the influence of GE on important aerodynamic parameters such as the lift and drag is well understood. For example, in an earlier study[5] for a M_∞=1.1 projectile it was found that the bullet was both attracted to (suction) and repelled from (lift) a solid surface. For a M_∞=2.4 projectile however, the projectile was found to only exhibit lift irrespective of the ground clearance[6] . This indicates that there exists an intermediate flow speed at which the projectile will no longer experience a suction force due to the presence of a solid surface. A similarly transition occurs for shock reflection patterns; for the transonic projectile all shock types that were exhibited were of the type mentioned above, while the supersonic projectile yielded only regular reflections. Through varying the two key parameters in GE analysis for projectiles, namely, ground separation distance h/d, and the freestream Mach number M_∞, a more complete understanding in this field may be gathered.

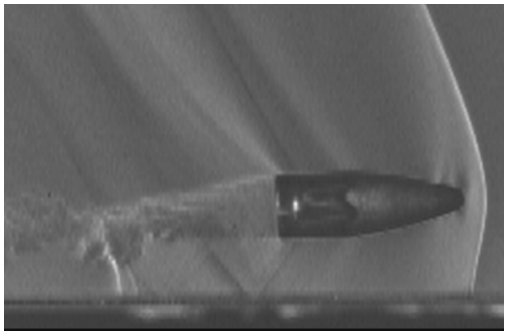

Figure 1: A live-fire schlieren image of a M_∞=1.1 projectile at a ground clearance of $h/d \approx 1.00$[1]

B. Guiding Theory

Ground effect is generally described as the phenomenan that occurs when two objects pass by one another in a fluid medium such that their respective flowfields are altered, leading to changes in aerodynamic behaviour. In most cases, one of objects is usually a plane ground surface. The influence of this effect is heavily dependent on a number of conditions, in particular the flow speed, the distance between the two objects, and finally their geometries. A primary design goal of any vehicle that flies or hovers is to achieve the highest possible $\frac{L}{D}$ ratio to improve its power requirements and efficiency. An aircraft in the proximity of one characteristic chord length will experience an effective increase in wing span - without the associated structural change or drag increase - as the surrounding flow shed from wing tip vortices and recirculation regions are compressed by the ground and spread outwards, creating a larger region of high pressure. In the context of land vehicles, GE is used in accordance with Bernoulli's principle for subsonic flow where the relative reduction of cross-sectional area (due to a cambered surface nearing the ground plane) causes

a pressure drop; thus, the resulting suction force may be used advantageously to improve the tyre grip on track[7] . In supersonic flow, GE is a result of reflected waves and their influence on regions of interest in the flowfield, in particular the subsonic zone surrounding the projectile, the pressure distribution along the surface, and the deflection/distortion of the wake.

In this study, three types of shock reflection cases have been observed and are shown in Fig. 2: Case *I* where the shock bends perpendicular to the ground plane and no reflection occurs; Case *II* where the angle of the deflected flow cannot be deflected parallel to the surface with a single reflected shock, thus the reflection point detaches from the surface to form a triple point and a Mach-stem is formed, and; Case *III* which is a regular reflection. To examine these cases, it is first required to understand the necessity for a reflected shock to exist within the flowfield. Consider the case where an incident shock created by a wedge at an angle θ is incident upon a flat surface. Shock-wave properties dictate that behind the shock the flow is inclined at an angle towards the wall; however, in order to preserve the wall boundary condition, the flow must be everywhere tangent to the flat surface[8] . In order for this to be possible, a second reflected shock is established at an angle relative to the wall, but different to the incident shock angle, that will deflect the flow such that it returns parallel to surrounding surfaces. The reflected shock sees a freestream Mach number that is lower than that seen by the incident shock, and thus the flow properties beyond the reflected shock are uniquely defined by the flow within the region between the incident and reflected shock.

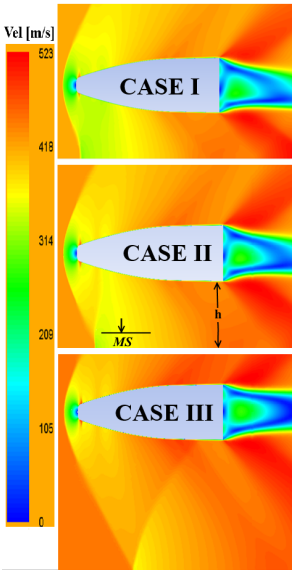

Figure 2: Examples of each shock reflection pattern for M_∞=1.2 at (top) $h/d = 0.85$, (mid) $h/d = 1.25$, and (bot) $h/d = 2.375$

Modelling transonic/supersonic GE inherently implies logistical complexities that include cost issues, resource availability, and at times military approval for range use. The two relatively cost-effective and primary methods for examining GE experimentally are the elevated ground plane and the symmetry (or dual model) method. The former must have its leading edge placed sufficiently far upstream such that any disturbances (*i.e.* shock waves) generated by the elevated ground, which must also be sufficiently far from the tunnel wall, do not impinge on the projectile[9] . Further, the introduction of a stationary ground that extends upstream of the projectile will create a boundary layer that does not exist in full-scale. The projectile is held by a wedge that extends above the model and may be adjusted for varying ground separation distances; though, this technique is limited to the wedge sizes available. The symmetry ground condition implements two identical models separated equidistantly by base-mounted sting fittings that slot into a double wedge holder. The upper model contains a force balance which allows the user to obtain measurements for lift, drag, and pitching moment. This method is effectively introducing an inviscid ground boundary which can be understood as an ideal reflecting surface.

This is advantageous as the intent of this technique is to eliminate the existence of a boundary layer,

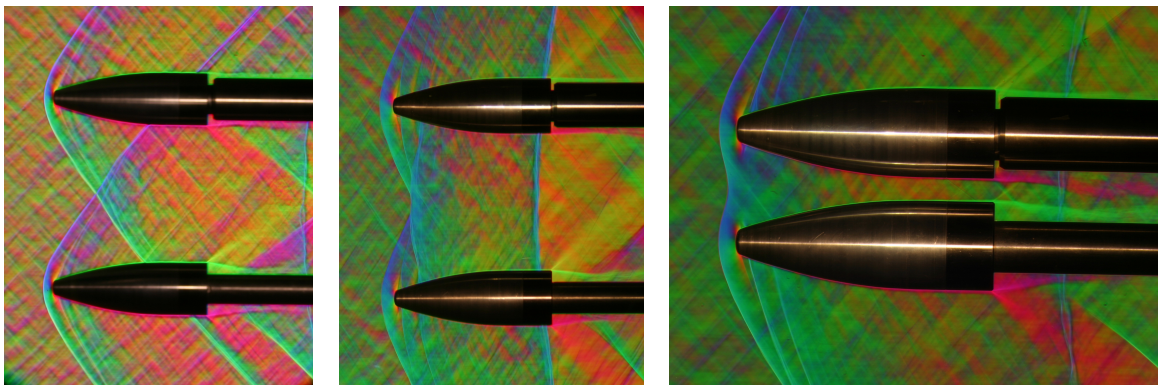

(a) (b) (c)

Figure 3: (a) Previous test: M=1.3 and h/d=1.25 (case *III* reflection), (b) recent test: M=1.2 and h/d=1.25 (case *II*), and (c) recent test with improved lighting on the projectile surface: M=1.3 and h/d=0.125 (case *I*)

which was shown in earlier studies to bend the shock wave such that the reflection strikes the projectile 6% further downstream then the symmetry method[10] . This is not entirely indicative of real-life however, as there are inherent differences in the way in which the reflected shock occurs; in the real-life flow the bow shock will reflect off a solid ground in quiescent air, whereas in the wind-tunnel for the symmetry case the interaction of the two reflected shocks will result in some form of mixing and diffusion of flow past the intersection point, albeit this is small. This mixing will further cause a shear layer to develop downstream of the shock interaction, though the overall influence that it has on the forces and moments experienced by the projectile in considered neglible. Colour schlieren was used to visualise the flow-field surrounding the projectile. This technique requires a carefully considered arrangement of spherical mirrors, slits, focal planes, and color filter assemblies that together enable the ability to visualise the transparent flow by detecting the respective magnitudes and directions of $\frac{\partial \rho}{\partial x}$ and $\frac{\partial \rho}{\partial y}$. A comparison of image quality from the most recent series of tests compared to those of a previous campaign is shown in Fig. 3. This method was developed by Kleine[11] and further information regarding the intracacies of this technique or variations thereof can be found in (Kleine, H. 2001).

II. Computational Approach

A. Outline of Numerical Method

A 64-bit commercial, finite-volume RANS solver (Fluent 14.5) was used for all simulations. A density-based, implicit coupled solver was combined with second-order upwinding to provide adequate steady-state solution accuracy. Spin of the projectile was neglected in this study as there is negligable difference shown between the spinning and non-spinning forces[5,10] . In order to simplify the model even further the rifling striations were also excluded. Extensive study has been undertaken to determine the effects of removing rifling grooves in the numerical analysis[12,13] of geometrically similar projectiles with results concluding the time and computational cost required for accounting for the small disturbances is not warranted and only margianally affect the yawing and the pitching moment coefficients. Excluding small disturbances assists the mesh generation as edge sizing around the model would require considerable attention and cells would need to be clustered in these areas to account for the very minor flow disturbances. The turbulent intensities and viscosity ratios were selected to be arbitrarily low values of 1% and 0.1 respectively for both the inlet flow and outlet. These values were deemed suitable for the model given that in real-life the projectile is in most cases encountering quiscent air. The simulations utilised first-order discretisation methods due to the complex nature of the wave reflections from the ground plane and high temperature and pressure gradients established over the projectiles surface. This was found to cause instability early in the simulations, and was overcome by implementing a method that has been successfully used[14] by beginning with a relatively low Courant number (between 0.8-1.2) that is progressively increased in value as the stability of the solution became evident, *i.e.* once shock reflections flowfield features are formed. The Courant number would be continuosly raised before the change of discretization method to second-order. All cases were run until changes in residuals, forces, moments, and inlet/outlet mass flow rates become negligible over a period of time (less than 0.1% over 500-1000 successive iterations). This approach was inherently very computationally expensive with individual simulations taking anywhere between eight to ten hours depending on the fidelity of the user during the process.

B. Model

The design specifications of the selected projectile (Nosler 50 *gn* S.H.O.T) for this study were unattainable commercially. The wind-tunnel model, initially manufactured and employed for testing at JAXA in 2009 to study the aerodynamic GE of transonic projectiles[1] , and again for wind-tunnel tests for this study, was selected for study once more. The dimensions of the scaled up model were measured digitally through image processing. The image was then uploaded to MATLAB where a smoothing function was applied to the data points obtained from the measurements. The data points were then imported into the ANSYS workbench environment which allows the user to define a suitable surrounding domain.

C. Mesh and Boundary Conditions

Boundary conditions are crucial to the accurate simulation of a CFD analysis and careful consideration must be given in order to determine how to represent the model. Projectile quarter-models are used to simulate out of GE, whereby the two planes that the projectile intersects are set as symmetry walls. The half-model is typically used for GE analysis with no spin, where the plane that intersects the projectile remains at symmetry and the ground plane is either set as a moving wall or symmetry. The boundary conditions used in this study are derived from the wind-tunnel experiments that were conducted at JAXA. As the model in the experiments used symmetry to model GE, the ground plane in the CFD simulations was enforced as a symmetry boundary condition. The outer domains of the volume were set as far-field boundaries to represent the walls at an infinite distance away from the model. This is not a true representation of the wind-tunnel as there were minor blockage effects present irrespective of how small the model is relative to the test section. The domain must be extended quite far radially as the far-field fluid boundaries in CFD are susceptible to reflecting shock waves. Thus for compressible flows, the domain must be sufficiently large such that the shock waves formed have space to dissipate and reflect off the far boundaries well beyond our region of interest. In transonic flow the shock waves are quite shallow, *i.e.* their reflections from the far-field boundaries are more likely to affect the region of interest, and subsequently require a very large domain in order to dampen and diffuse[15] . As the flow speed increases into the supersonic region the Mach angle μ decreases and thus the domain can be progressively reduced in size to reduce computational cost.

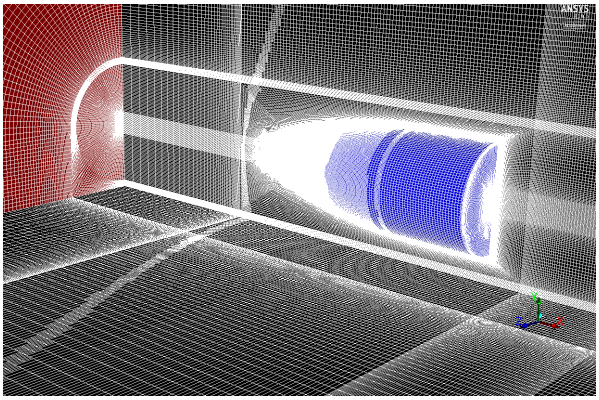

(a) Indication of surfaces

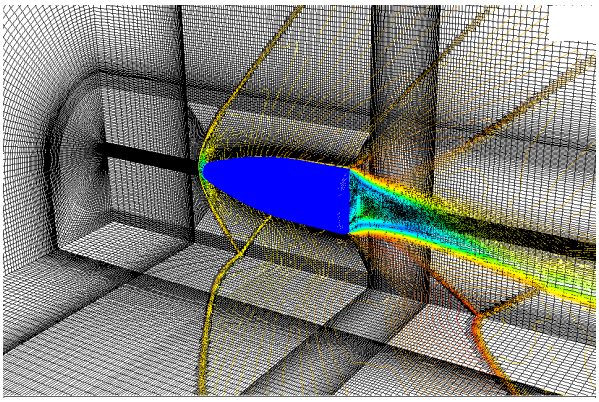

(b) Velocity contours highlighting the mesh adaptation of cells surrounding regions of high pressure gradients such as shock waves

Figure 4: An example of the domain types used in (a) $h/d \leq 0.85$ and (b) $h/d \geq 1.00$. Note that in (a) the red surface designates a *pressure inlet*, the black surfaces are that where symmetry is imposed, and the blue indicates a solid wall.

As no formal study was conducted by the author on the sensitivity of the results to varying domain size, this present study focussed on a domain that extended one projectile length upstream and between 10-12 projectile lengths both downstream and radially depending on the flow regime used. Domain size variations and the implications that it has on the projectile has been examined[6] for a quarter-model travelling at $M_\infty = 2.4$ out of GE with results showing that the most appropriate domain extended 11 projectile lengths downstream and six lengths radially. The domain size underneath the projectile will change for varying ground separation clearances. Figure 4 illustrates the domain configurations used in this study for $h/d \leq 0.85$ and $h/d \geq 1.00$.

For this study, the greater domain was resolved into a number of smaller volumes utilising a combination of both slice and boolean operations. The geometry was constructed in this way to allow controlled edge sizing, mapped face meshing, and sweep methods within the solids to ensure a consistent and cleaner element transition between each section. This approach ensured that the mesh was made fine with cells clustered in regions where complex flow features and high viscosity exist, *i.e.* immediately surrounding the projectile surface, near-base wake, and the ground plane. This aided the visualisation of the boundary layer and shock interactions. The meshing strategy implemented came at the cost of the inability to utilise typical y^+ optimisers such as first cell heights and inflation layer thicknesses due to the problems with mesh generation; thus, an alternative approach was used whereby the mesh was constructed and the y^+ was refined later in the solution process. The computational cost became increasingly expensive with each successive adaption, thus it was decided following a y^+ dependency study that a $y^+ \leq 5$ was sufficient.

D. Turbulence Model Study

1. *Description and Review*

Military projectiles are typically used at very low altitudes under immense dynamics conditions. They are usually designed with a surface finish that encourages the immediate transitioning of the flow into turbulent[16] There are a number of turbulence models that may be suitable for the computational analysis of this study; however they must be evaluated against each other with respect to their ability to reproduce the experimental flow-field behaviour. In order to select the most appropriate model, a comparison of three similar RANS turbulence models has previously been conducted in the transonic[5] and supersonic[6] $M_\infty = 2.4$ regimes; in both cases the more challenging (in terms of flow complexity) ground separation distance of $h/d = 0.5$ was used for comparison. Pressure distributions along the length of the projectile for $h/d = 0.5$ for each of the respective models were compared to wind-tunnel tests in order to determine the model choice for the study. The upper surface for all cases strongly correlated to the data seen for a projectile for the no ground case; this is due to negligible GE influence on the upper surface as the shock interactions that occur with the projectile body are pertinent mainly to the lower surface. As a result of this correlation for the upper surface, it can be deduced that these models are appropriate for comparison to the lower surface results. The differences on the lower surface were not significant enough to warrant the selection of any model, thus the k-ω model was selected based on its accuracy for transonic flows and its advantageous use for modeling flow separation and free shear layers. This was due to the important flowfield features such as shock interactions seen in experiments at this height. In these instances, the RANS turbulence models that were used for evaluation were the Spalart-Allmaras (SA) 1-equation model[17] , the SST variant of the k-ω model[18] , and the realisable k-ϵ model[19] . Each model has inherent issues when dealing with compressible flow, for example, the SA model has difficulty handling and is scarcely used for problems involving large scale vortices and recirculation zones; k-ϵ has shortfalls in its ability to accurately model flows where separation occurs, and the standard k-ω is the opposite in that it is more suitable for near wall effects. The SST k-ω is essentially a combination of the two aforemoentioned models as it is able to use their best characteristics for the appropriate location in the flowfield.

2. *Selection of Model*

Depsite previous studies with the same projectile model citing the two equation SST k-ω model as the most suitable for this research, it was necessary to conduct an independent study. Selection was determined based on qualitative flowfield comparisons with experimental tests, surface pressure distribution, aerodynamic forces, shock impingement location, and convergence time. Fig. 5 illustrates the pressure coefficient along the top and bottom surface for the $M_\infty = 1.3$ and h/d=1.25 case. The models present almost identical distributions except for at x/l≈0.55-0.58 which correlates to the shock impingement location for this particular flight regime. The distribution indicates that all models predict the reflected shock will impinge at almost the same location, however a comparison of the CFD and colour schlieren images reveals that the Spalart-Allmaras model underpredicts the experimental result by 6.5%, while the SST k-ω model yields the most accurate prediction at 4.5%. Further downstream beyond the shock reflection, there were no further notable differences for both the pressure and velocity contour plots in the near projectile flowfield. Despite the SA model solving one less equation during the iterations, it did not appear to converge at a faster rate then the two-equation models. All solutions converged within 4000 iterations at a equivalent rate with continued monitoring of the Courant number and grid refinements made during the solution process. The SST k-ω compared favourably to the SA model for lift and moment, and realisable k-ϵ for drag. As the other two models did not yield comparable results with each other, and in conjunction with the more refined shock impingement location, the SST k-ω was considered most suitable for undergoing this study.

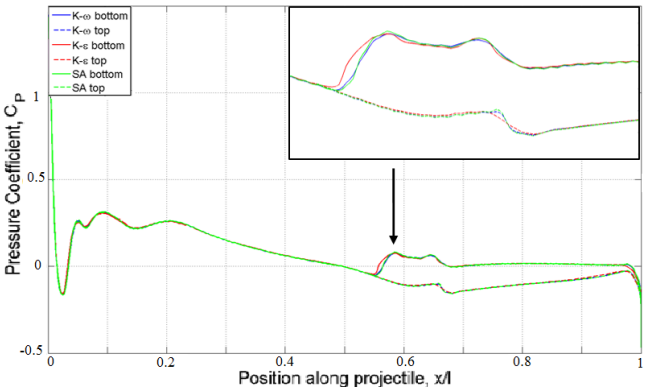

Figure 5: Pressure distribution comparison of the turbulent models examined in this study for $M_\infty = 1.3$, $h/d = 1.25$

E. Verification and Validation

1. *Grid Independence*

Grid independence was adjudicated both quantitatively and qualitatively. The aerodynamic forces and moments for each level of pressure gradient cell adaptation are presented in Table 1, where the variation in lift, drag and moments are all in the vicinity of 0.5% and 0.05% for the first and second refinements respectively. This suggests that the standard mesh is sufficient for obtaining the force and moment measurements. The downfall with the standard mesh, however, is that the shock resolution in the aforementioned key regions is inadequate, particularly for differentiating between Mach and regular shock reflection patterns for low Mach-stem heights. A mesh with cell adaptation across a pressure gradient of 1000 *Pa* was selected over the standard model. This increased the convergence time on average from approximately 6 to 9 hours per simulation.

Gradient [Pa]	Lift [N]	Drag [N]	Mom. [Nm]	Cells
Mach 1.2, h/d = 1.25				
-	4.565	30.709	0.314	3501800
1000 Pa	4.533	30.608	0.312	4303600
2000 Pa	4.532	30.616	0.311	5196100
Mach 1.4, h/d = 1.00				
-	7.891	27.622	0.141	2688000
1000 Pa	7.879	27.369	0.139	3203000
2000 Pa	7.877	27.327	0.139	4037000

Table 1: Mesh refinement study for two different flight conditions, comparing the quantitative results for the standard mesh with two cell adaptations employed across high pressure gradients

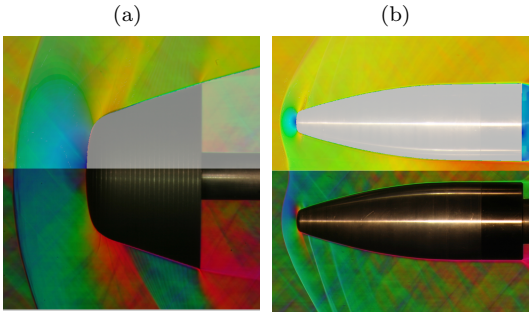

Figure 6: Comparison of (top) CFD velocity contour and (bot) colour Schileren wind-tunnel tests for no ground and case *I*

2. *Verification of Results*

Figure 6 compares the numerical and wind-tunnel results for two of the observed flight conditions exhibited in this study, *i.e.* a no ground case (single model) and a case *I* shock reflection pattern where the shock bends forward and strikes the ground perpendicularly, forming a normal shock. The no ground comparison illustrates the identical bow shock curvature and shock stand-off distance, with the wind-tunnel result yielding the expected slightly larger stand-off due to blockage effects. The case *I* comparison shows that the shocks are found to interact at the same location on the imaginary ground plane. The only notable difference between the numerical and colour schlieren images are where the shock reflection angle (for case *III* shocks) in the numerical model is slightly curved towards the projeciles ogive forebody, whereas the experimental result yields an almost unaffected shock with negligble deviation. It was found that the aerodynamic forces and moment, particularly drag, were strongly dependent on the configuration of the domain and mesh used. A comparison of the results by Carriage (2012) and Doig (2010) has been conducted to illustrate that the results from this study are reasonable (see Fig. 7). Despite minor differences ($< 10\%$) in both parameters, the general shape and behaviour of the curves remain the same.

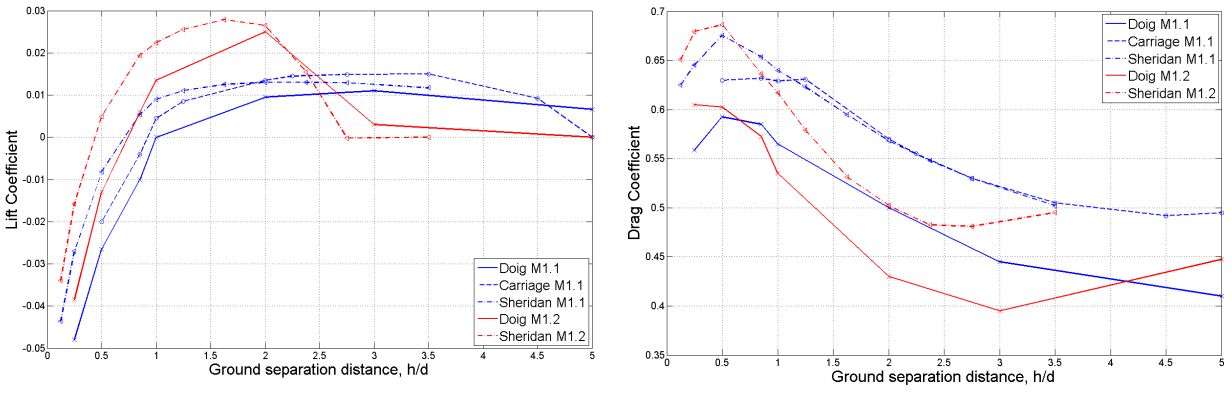

(a) (b)

Figure 7: Comparison of results with previous studies conducted by Carraige (2010): $M_\infty = 1.1$ and Doig (2010): $M_\infty = 1.1$ and 1.2 for lift and drag

III. Results and Discussion

A. Forces and Moments

1. *Lift and Drag*

THE lift and drag coefficients once the projectile is in close proximity to a solid surface are shown in Fig.8. A number of trends are evident with increasing Mach number, namely; the region of influence of h/d is reduced; the peak C_L both increases and translates left to a closer ground clearance, and; the magnitude of the suction force at the smallest h/d decreases at an appreciably larger rate. For all Mach regimes tested the projectiles sensitivity to h/d, $\frac{dC_L}{dh/d}$, was greatest immediately beyond $h/d = 0.125$. Importantly, once $M_\infty = 1.5$ the suction force was no longer experienced.

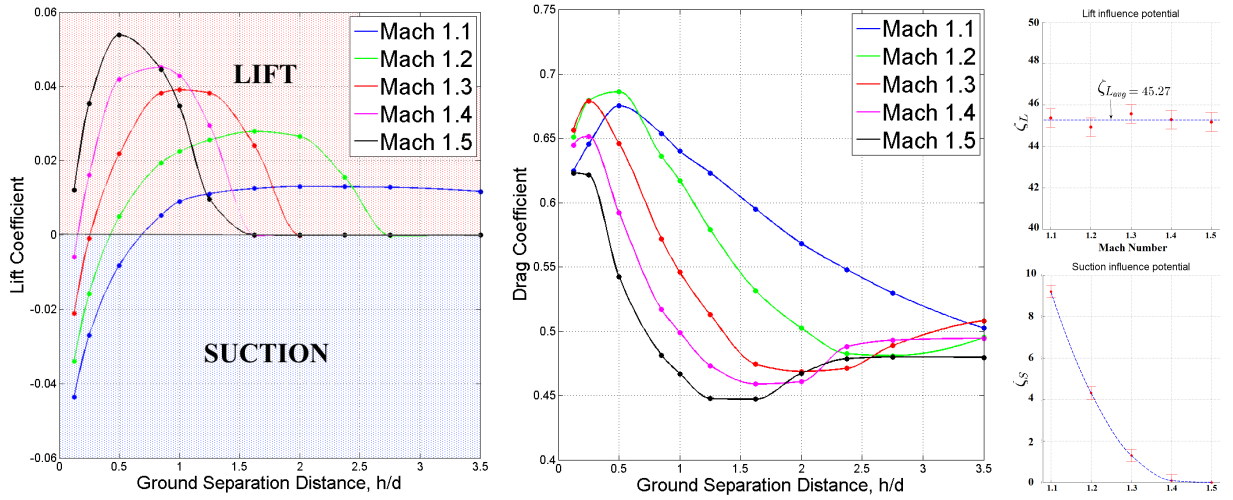

(a) (b) (c)

Figure 8: (a) lift and (b) drag coefficient vs. ground clearance for the Mach range of $M_\infty = 1.1$–1.5, and (c) the lift (top) and suction (bot) influence potential of ground plane

In addition to these physical features, integration of the curves both below and above $C_L = 0$ yielded a parameter that can be interpreted as the ground influence potential, ζ. For the positive area, *i.e.* above $C_L = 0$, the ζ_L parameter describes the lifting potential that the solid surface may induce on the projectile over the range of separation distances in GE. Similarly its counterpart, ζ_S, describes the suction potential of the solid surface. It was found that ζ_L is approximately constant over the Mach regimes tested in this study; subsequently, the lifting influence of the ground plane while the projectile is in GE for transonic/low supersonic flows is independent of the projectiles speed. More importantly, from the range of cases tested it can be suggested that a lifting potential will always exist regardless of the Mach number. The suction influence potential of the ground revealed an expected trend in that ζ_S reduces with increasing Mach number. After M_∞=1.5, suction no longer exists for the lowest feasible ground clearance considered.

The complex shape of the drag curve is attributable to its high sensitivity to the complex physical flow-field features. Immediately beyond the lowest ground clearance there is a drag peak with a magnitude and width that decreases with an increase in Mach number. Upon reaching M_∞=1.5, this peak no longer existed as a plateaued region developed, albeit only for the range of $0.125 \leq h/d \leq 0.250$. Following the peak, all curves exhibited a significant drop in drag with the steepness becoming larger for higher Mach numbers, resulting in the local minimum occurring at lower h/d locations; this is largely due to where the reflected shock impinges on either the projectile or wake. Viscous forces were found to have a negligible change when the reflection struck the projectile, therefore the primary driver for the changes in total drag are the effect that the shock reflections have on the pressure and wake drag, *i.e.* any distortion, deflection, or combination of both, of the wake. For low ground clearances the wake, which is bounded by a shear layer that encapsulates the flow, thickens immediately downstream of the base and is pulled towards the ground due to the large concentration of low pressure constrained between the wake and the solid plane. This results in a non-linearly behaving interaction of two low pressure recirculation regions within the wake, which are no longer symmetric about the projectile lengthwise axis as one tends to compress the other, depending on the direction of wake deflection.

2. *Ground Effect Flight Configurations*

There are four possible lift/moment configurations that may be experienced by a projectile in GE and they are summarised in Table 2, along with the demarcation of those conditions for $M_\infty = 1.2$ to 1.5 in Fig.9. The region over which the three primary GE flight configurations occur decreases with increased Mach number, such that once $M_\infty = 1.5$ *A* is no longer experienced by the projectile. A similar trend appears to be occuring for condition *B*, such that there may exist a flow speed where only *C* and *D* occur in GE. These flight configurations are important beyond the steady-state phase examined in this study as they are primary indicators of the potential behaviour of the projectile in its flight trajectory.

B. Flowfield

1. *Bow-shock and Stand-off Distance*

The relationships presented in Fig. 10 depicts the strong dependency between shock stand-off ratio, SD/d, and the ground separation ratio, h/d, particularly for lower Mach numbers. $M_\infty = 1.2$–1.4 are presented with the same scale to highlight both the magnitude of increase of SD/d and the size of the region that it is affected by the ground plane. The maximum $\Delta SD/d$ between the $h/d = \infty$ and GE cases for M_∞=1.1 to 1.3 are +68%, +26% and +4% respectively, with a negligible change shown for M_∞ and beyond. The value of SD is mainly influenced by the vertical extent of the volume occupied by the subsonic zone. The subsonic zone is presented for three ground clearances for M_∞=1.2 and 1.3 in Fig.10. It is clear that the volume decreases with increasing ground clearance. A similar trend occurs for fixed h/d with increasing M_∞. As mentioned earlier, a shock is unable to reflect from a surface unless the surrounding region is locally supersonic; thus, as both the Mach number and h/d increase the volume occupied by the subsonic zone tends towards the no ground condition where the region of subsonic flow behind the bow shock is axisymmetric about the axis of the projectiles length.

2. *Shock Reflection Cases and Mach-Stem Height*

Shock reflection cases were determined by visual inspection on the z=0 plane. In order for case *II* to be assigned, the Mach-stem must have been both distinguishable on the pressure and velocity contour plots, and have a stem height such that $MS/h > 0.05d$ to remove any potential ambiguity when differentiating between case *II* and *III*. A summary of the expected demarcation of the three shock reflection cases, and an example of each, is shown in Fig. 2 and Fig. 11 resepectively. Mach 1.1 is shown to only yield case *I* reflections where the shock bends forward to meet the ground perpendicular. It is likely that this will continue beyond h/d>3.5 as the bow shock will have diffused to the extent where there will be no reflection at all.

Condition	Lift	Moment
A	-	-
B	+	-
C	+	+
D	0	0

Table 2: Force/moment configurations while in GE. Note that *+ve* indicates lift force and pitching moment nose up

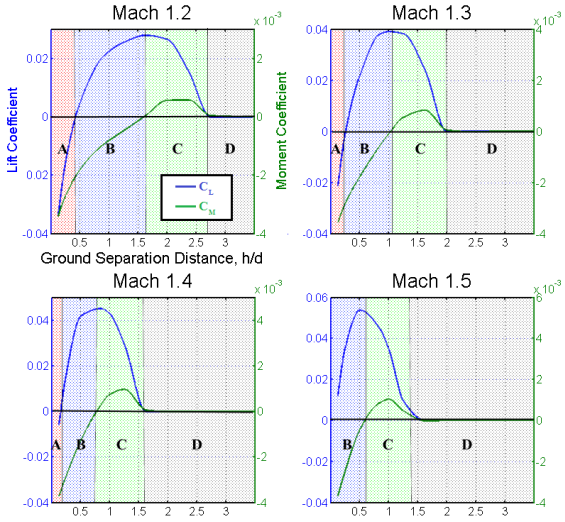

Figure 9: Lift/moment curves to illustrate the flight regimes that exist for a given Mach number

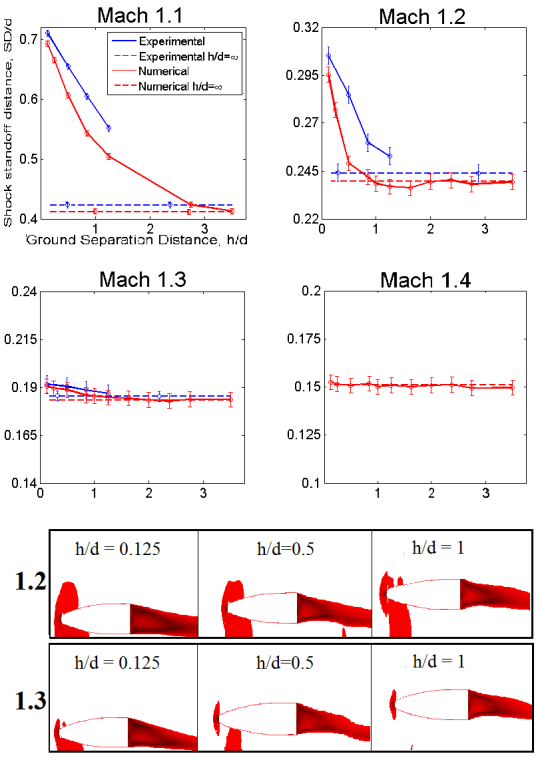

Figure 10: Experimental and numerical results of shock stand-off distances SD/d for M=1.1–1.4 over $0.125 \leq h/d \leq 3.500$. Below: Subsonic zones for Mach 1.2 and 1.3 at h/d=0.125, 0.5 and 1.

From the expected dermarcation of cases there is a theorised region of shock pattern instability that occurs in the vicinity of $M_\infty = 1.1$–1.2 and $h/d>2$ where the shock reflection type is extremely sensitive to any change in flight conditions and is thus it can be conjectured that all patterns simultaneously occur. Case *I* reflections are found to no longer occur for $M_\infty \geq 1.4$; this is a manifestation of the subsonic zone immediately downstream of the bow shock reducing in size such that it no longer makes contact with the solid surface, thus forming a case *II* reflection.

The *II*→*III* transition beyond $M_\infty > 1.5$ is unclear; though, it should be noted that a similarly shaped projectile at $M_\infty = 2.4$ was examined by Doig *et al.* (2010) and case *III* reflections were found to occur at ground clearances as low as $h/d = 0.2$. This may suggest that for objects which are geometrically similar to a projectile, there may exist a physical limit for the occurence of Mach reflections. The height of the Mach-stem *MS* relative to the projectile ground clearance was found to vary with both Mach number and h/d. The stem height was found to be at a maximum immediately after transition from case *I*→*II* reflection occured, and then decreased as the location of the triple point moved further downstream. Note that h in this study is the height above the ground for the location of the projectiles largest diameter, *i.e.* the base. This then allows the possibility for $MS/h>1$, as a particular condition may result in the stem extending above the reference h line into the volume in the front of the ogive forebody.

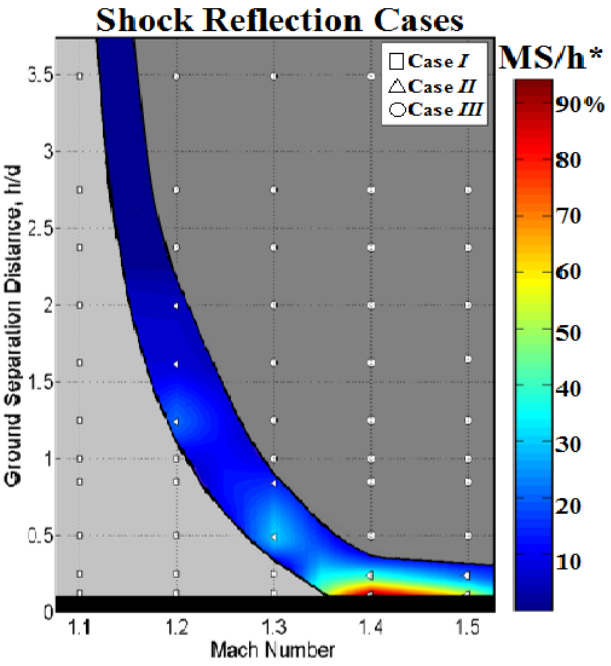

Figure 11: Expected dermarcation of shock reflection cases determined from the numerical and experimental data

3. *Pressure Distributions*

The pressure distributions for various clearances along the projectile length x/l on the axial $z=0$ plane are presented in the form of a pressure coefficient. As the ground clearance is increased the bow shock reflection is naturally weakened and becomes more susceptible to being influenced by the expansion fans that form around the forebody. As the ground clearance increases the expansion waves diffuse and no longer influence the projectile. The bow shock reflection however, continues to cause a region of high pressure which contributes to the projectile pitching moment behavior depending on where the shock strikes the surface. At low clearances the subsonic zone on the top surface occupies more volume and extends further along the projectile length, thus affecting the distribution along the ogive forebody. The top surface returns to its no ground state at a smaller clearance than the bottom surface as the features of the shock regardless of its type are no longer able to wrap around the body.

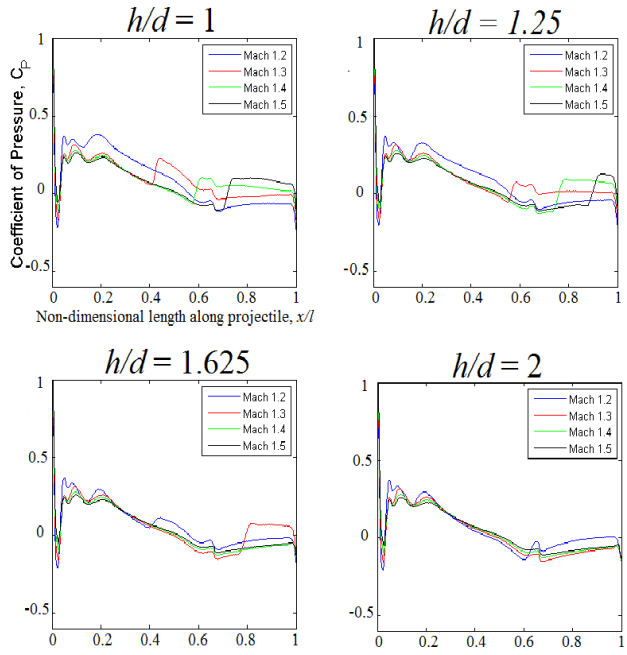

Figure 12: Pressure distribution on the projectile bottom surface ($z=0$) as a function of Mach number and ground clearance

A comparison of the pressure distribution along the bottom surface for ground clearances $1.000 \leq h/d \leq 2.750$ is presented in Fig. 12. The pressure change immediately downstream of the reflected shock impingement

increases with Mach number, which correlates to the results shown in Fig. 8(a) where the peak magnitude of the lift coefficient is shown to similarly rise. The reflected shock impingement location on the bottom surface is clearly shown to transition aft with an increase in ground clearance. Further, the h/d at which the reflection begins to interact with the wake becomes evident once the curve returns to its ground state. This is shown to occur at a clearance $1.250 \leq h/d \leq 1.625$ for $M_\infty > 1.4$. The h/d at which shock-wake interaction initially occurs is important as it substantially contributes to the overall drag increase beyond the local drag minimum shown in Fig. 8 (b).

IV. Conclusions

A range of ground clearances and Mach numbers were investigated to determine the qualitative and quantitative influence of GE once a projectile travels within close proximity of a solid plane. It was found that the amount of lift that the ground plane could induce on the projectile while in GE was independent of Mach number for low supersonic, whereas the suction potential decreased beyond $M_\infty = 1.1$ such that suction no longer existed once $M_\infty = 1.5$. A drag peak occurs beyond the smallest ground of h/d=0.125 which becomes less appreciable as Mach number is increased.

There are three different lift/moment configurations observed while in GE; Conditions *A* (suction, pitch nose up), *B* (lift, pitch nose up), and *C* (lift, pitch nose down). As Mach number increased their region of occurence decreased such that for $M_\infty = 1.5$ condition A was no longer shown, with *B* similarly reducing in size. The bow shock stand-off distance was found to have a maximum $\Delta SD/d$ between the h/d=∞ and GE cases of +68%, +26%, and + 4% for $M_\infty = 1.1$–1.3 respectively. This is largely driven by the subsonic zone that occupies the volume surrounding the blunt nose and ogive forebody. The vertical extent of this zone reduces with increasing Mach number such that it can no longer interact with the ground plane, and thus pushes the shock forward of its out of GE location. The subsonic zone was also found to strongly influence the shock reflection pattern.

A case *I* reflection was found to occur for $M_\infty < 1.4$. Case *II* reflections occupied a thin band that existed between case *I* and *III* and resulted in a region bounded by $1.1 \leq M_\infty \leq 1.2$ and $2.25 \leq h/d \leq 3$ where the shock reflection pattern that occurs will be extremely sensitive to any variation in either parameter, thus in that region it is conjectured that all patterns simultaneously occur. The Mach-stem height for case *II* reflections was found to peak for low ground clearances at higher Mach numbers. The non-linear behaviour of the wake being pulled towards and deflected away from the ground was found to be a significant contributor to the drag as the recirculation zones in near-base region deflected and distorted the wake.

V. Recommendations

There are two obvious avenues for any continuation of this work. Firstly, a transient study that examines how the flowfield develops from the moment a projectile encounters a solid plane into its steady-state solution. If this portion of the study is to be fulfilled by an undergraduate user in the future it is recommended that they have extensive CFD knowledge before beginning the project. Secondly, the expected demarcation of shock reflection patterns has been shown for the Mach and ground clearance ranges examined. In order to fully understand the behaviour of the shock reflection cases, further refinement is necessary along regions where the demarcations have been indicated by the author, in particular surrounding the region of high sensitivity. As a result of this refinement, additional information may also be obtained regarding the Mach-stem height *MS/h*.

Acknowledgements

My deepest gratitude is given to A/Prof. H. Kleine and A/Prof. J. Young, my undergraduate thesis supervisors. Their unparalleled passion towards research provided me with the motivation to exceed beyond what I thought was possible. A special thanks is also extended to the Japan Aerospace Exploration Agency, Sagamihara, Japan, for hosting our wind-tunnel test campaign in May 2014. Although this was not explictly a core component of my research, the experiences had were fundamental in guiding me towards the completion of my thesis. Lastly, to my family and friends, I thank you for your incredible patience and understanding over the duration of this research.

References

[1]Oakes, B. J. W. Aerodynamic ground effect of transonic projectiles. *BE Thesis, School of Engineering and IT, UNSW@ADFA, Canberra*, 2009.

[2]Purdon, J. P., Mudford, N. R. and Kleine, H., Supersonic projectiles in the vicinity of solid surfaces *Proceedings of the 27th International Congress on High Speed Photography and Photonics*, vol. 6279, SPIE, Bellingham, pp.1–8, 2007.

[3]Torda, T. P. and Morel, A. T. Aerodynamic design of a land speed record car. *Journal of aircraft*, **8**(12): pp.1029–1033, 1971.

[4]Kell, R. T. Aerodynamic analysis of F1 in schools cars. *BE Thesis, School of Engineering and IT, UNSW@ADFA, Canberra*, 2009.

[5]Carriage, K., Young, J., Kleine, H. and Hiraki, K. Reynolds-Averaged Navier-Stokes computation of transonic projectiles in ground effect. *18th Australasian Fluid Mechanics Conference, Launceston, Australia, 3-7 Dec*, 2012.

[6]Doig, G., Barber, T. J., Leonardi, E., Neely, A. J., and Kleine, H. Aerodynamics of a supersonic projectile in proximity to a solid surface. *AIAA Journal*, **48**(12): pp.2916–2930, 2010.

[7]Katz, J. Aerodynamics of race cars *Annual Review of Fluid Mechanics*, vol. 38, pp.27–63, 2006.

[8]Anderson, J. D. Jr. Fundamentals of aerodynamics, 5^{th} ed. *McGraw-Hill*, 2009

[9]Doig, G., Barber, T., Leonardi, E., Neely, A. J., and Kleine, H. Methods for investigating supersonic ground effect in a blowdown wind tunnel. *Shock Waves*, **18**(2): pp.155-159, Jun 2008.

[10]Doig, G., Barber, T. J., Leonardi, E., Kleine, H., Neely, A. J., Purdon, J. P., Appleby, E. M., Mudford, N. R., The aerodynamics of a supersonic projectile in ground effect. *Proc. ISSW26*, vol. 2, Springer, pp.1521–1526, 2009.

[11]Kleine, H. 5.1. Flow visualisation: Measurement techniques and diagnostics. *Handbook of Shock Waves*, Academic Press, San Diego, Vol. 1, 2001

[12]Silton, S. and Webb, D. Experimental determination of the effect of rifling grooves on the aerodynamics of small caliber projectiles. *AIAA Atmospheric Flight Mechanics Conference and Exhibit, Keystone, CO*, 21-24 Aug, 2006.

[13]Weinacht, P. Validation and prediction of the effect of rifling grooves on small caliber ammunition performance. *AIAA Atmospheric Flight Mechnanics Conference and Exhibit, Keystone, CO*, 21-24 Aug, 2006.

[14]Silton, S. Navier-Stokes computations for a spinning projectile from subsonic to supersonic speeds. *Journal of Spacecraft and Rockets*, **42**(2): pp.223–231, 2005.

[15]Sahu, J. Numerical computations of transonic critical aerodynamic behaviour. *U.S Army Research Laboratory, Aberdeen Proving Ground, MD*, pp.299–316, 1988.

[16]Sturek, W., Nietubicz, C. and Weinacht, P. Applications of computational fluid dynamics to the aerodynamics of army projectiles. *Journal of Spacecraft and Rockets*, **31**(2): pp.186–199, 1994.

[17]Spalart, P. and Allmaras, S. A one-equation turbulence model for aerodynamic flows. *AIAA Aerospace Sciences Meeting and Exhibit, Reno, NV*, AIAA-92-0439, 6-9 Jan. 1992.

[18]Shih, T., Liou, W. W., Shabbir, A., Yang, Z. and Zhu, J. A new k-ϵ eddy viscosity model for high reynolds number turbulent flows model development and validation. *Computers and Fluids*, **24**(3): pp.227–238, 1995.

[19]Menter, F. R. Two-equation eddy-viscosity turbulence models for engineering applications. *AIAA Journal*, **32**(8): pp.1598-1605, 1994.

[20]Doig, G., Barber, T. and Neely, A. Progress in understanding transonic and supersonic ground effect aerodynamics *28th International Congress of the Aeronautical Sciences*, 2012